PAPER

Check for updates

Pressure-swing absorption and desorption behaviours of ammonia in bis(trifluoromethylsulfonyl)amide salts†

Manabu Tokushige, Ryota Fujisawa and Junichi Ryu 🆔 *

The absorption and desorption behaviours of NH_3 in bis(trifluoromethylsulfonyl)amide (TFSA) salts were investigated using the pressure-swing method. The effects of cation species and temperature on the NH_3 absorption behaviour of four TFSA salts, namely, Na[TFSA], K[TFSA], Mg[TFSA]$_2$, and Ca[TFSA]$_2$, were evaluated. NH_3 was absorbed by these solid TFSA salts, and high NH_3 desorption was observed for Na[TFSA] at 473 K and K[TFSA] at 300 K. The NH_3 absorption behaviour varied with the cation of the TFSA salt. Crystallographic refinement showed that the crystal lattice of Na[TFSA] expanded and contracted along the c-axis upon NH_3 absorption and desorption, respectively, indicating the coordination of NH_3 molecules with cation sites between the lattice layers. For the alkaline-earth metal TFSA salts, NH_4[TFSA] and amide compounds (Mg(NH$_2$)$_2$ or Ca(NH$_2$)$_2$) were formed after NH_3 absorption. Therefore, two absorption processes—coordination and dissociation of NH_3—occurred in the TFSA salts.

1 Introduction

For over a century, ammonia (NH_3) has been produced, addressing food security as a nitrogen-based fertilizer and securing our livelihood by serving as a feedstock for various chemical products.[1,2] However, conventional production (*via* the Haber–Bosch process) requires a substantial amount of energy because of the requirement of high pressures (5–20 MPa) and temperatures ranging from 673 to 873 K for the synthesis of NH_3.[1–7] In contrast, Aika *et al.*[8–11] proposed an NH_3 production system using a Ru catalyst and selective NH_3 absorber. Conventional separations of NH_3 involve cryogenic condensation below 240 K,[12–14] even though NH_3 is obtained from the synthetic reactors at high temperatures (~473 K).[15,16] The cryogenic condensation of high-temperature gases containing NH_3 and reactants (H_2 and N_2) requires a substantial amount of energy, and the subsequent reheating to return the reactant gases to the synthetic reactor results in energy loss.[10,11,17–19] The selective NH_3 absorber reduces energy losses during NH_3 separation, and swift NH_3 separation using absorbers enables the synthesis of NH_3 under mild conditions such as lower pressures and temperatures because the production rate of NH_3 is improved by the prompt circulation of reactant gases.[11,17–23] Liu and Aika[18–20] confirmed that mixed halide compounds such as $CaCl_2$ and $CaBr_2$ exhibited a high NH_3 storage capacity and established the production system for NH_3 using these

absorbers (the absorber-enhanced Haber–Bosch process). Malmali *et al.*[24–31] demonstrated that NH_3 was economically and efficiently produced using the absorber-enhanced Haber–Bosch process. They separated NH_3 using halides as the absorber at 453 K and 0.6 MPa and confirmed that the production of NH_3 was determined by the circulation rate of reactant gases. The absorber-enhanced Haber–Bosch process reduces the cost and energy consumption required to produce NH_3. Although various types of absorbers have been investigated,[17–41] the operation of the absorber-enhanced Haber–Bosch process has still not been optimized because of the complex NH_3 absorption and desorption mechanisms, such as the discrete stoichiometry of ammine compounds and slow NH_3 desorption.[37] NH_3 is absorbed into halides through the coordination of NH_3 with the cation and formation of ammine complexes. Subsequently, it desorbs from halides by dissociation of ammine complexes and diffusion of NH_3 into the gas phase.[19] The formation and dissociation of ammine complexes are relatively slow. The rates of formation and dissociation of ammine complexes are predominantly determined by the heat of reaction (enthalpy change), which serves as the energy barrier for the absorption and desorption of NH_3. The dissociation of many ammine compounds requires a substantial heat of reaction (~100 kJ mol^{-1}) (Table 1), resulting in a low NH_3 desorption rate. This implies that the rate and efficiency of NH_3 production are enhanced by improving the NH_3 desorption function of the absorber. Malmali *et al.* desorbed NH_3 from an absorber using the temperature-swing method (TSA). Meanwhile, we have developed a high-temperature NH_3 absorber to separate NH_3 obtained at 473 K from the synthetic reactor. This selective absorber reduced the heat loss during cooling and reheating

Graduate School of Engineering, Chiba University, Chiba 263-8522, Japan. E-mail: jryu@chiba-u.jp

† Electronic supplementary information (ESI) available. See DOI: https://doi.org/10.1039/d4se00820k

Table 1 NH_3 absorption functions of each absorber at the standard state

Absorber	Ammine compounds	Storage capacity	Enthalpy change	Reference
$MgCl_2$	$Mg(NH_3)Cl_2$	11 mmol g^{-1}	−93 kJ mol^{-1}	32
	$Mg(NH_3)_2Cl_2$	21 mmol g^{-1}	−85 kJ mol^{-1}	
	$Mg(NH_3)_6Cl_2$	63 mmol g^{-1}	—	
$CaCl_2$	$Ca(NH_3)Cl_2$	9 mmol g^{-1}	−81 kJ mol^{-1}	
	$Ca(NH_3)_2Cl_2$	18 mmol g^{-1}	−74 kJ mol^{-1}	
	$Ca(NH_3)_4Cl_2$	37 mmol g^{-1}	−83 kJ mol^{-1}	
	$Ca(NH_3)_8Cl_2$	72 mmol g^{-1}	−164 kJ mol^{-1}	
$CaBr_2$	$Ca(NH_3)Br_2$	5 mmol g^{-1}	−71 kJ mol^{-1}	
	$Ca(NH_3)_2Br_2$	10 mmol g^{-1}	−79 kJ mol^{-1}	
	$Ca(NH_3)_6Br_2$	20 mmol g^{-1}	−182 kJ mol^{-1}	
	$Ca(NH_3)_8Br_2$	40 mmol g^{-1}	−83 kJ mol^{-1}	
[emim][TFSA]	—	42 mmol g^{-1} @ 1.0 MPa	−7 kJ mol^{-1}	33

NH_3 and reactant gases, as NH_3 is easily separated using the pressure-swing method (PSA). Bis(trifluoromethylsulfonyl) amide (TFSA) salts, which are amide salts with imino groups, have several desirable properties such as nonvolatility, nonflammability, high thermal stability, absorption of NH_3, and low solubilities of H_2 and N_2.[42–55] For example, NH_3 dissolved in 1-ethyl-3-methyl-imidazolium ([emim]) [TFSA] at 300 K has solubilities of 42.3, 3.36, and 0.527 mmol g^{-1} at 1.0, 0.4, and 0.1 MPa, respectively.[33] The heat of dissolution of NH_3 in this TFSA salt (~10 kJ mol^{-1}) is lower than that required for the formation of ammine complexes (~100 kJ mol^{-1}), which indicates that the rates of absorption and desorption of NH_3 in this TFSA salt are higher than those in halides. Furthermore, TFSA$^-$ anions can interact with metal centers either as bidentate ligands or by bridging several metal centers.[56] Consequently, alkaline and alkaline-earth metal TFSA salts exhibit layered structures in the solid state, as shown in Fig. 1.[56–59] Because the NH_3 molecule coordinates with a cationic site,[19,23] these solid TFSA salts are expected to absorb NH_3 molecules at each cationic site between the lattice layers. In this study, we investigated the absorption/desorption behaviour of NH_3 in solid TFSA salts at 473 and 300 K. For four TFSA salts, namely Na[TFSA], K[TFSA], Mg[TFSA]$_2$, and Ca[TFSA]$_2$, the effects of cation species and temperatures on the NH_3 absorption behaviour were evaluated using crystallographic and kinetic analyses.

2 Experimental

The NH_3 absorption/desorption cycles of the four TFSA salts were measured using a magnetic suspension balance (MSB-143, Rubotherm GmbH, Germany) and the pressure-swing method. Commercially available TFSA salts such as Na[TFSA] (purity: >98%; SO989), K[TFSA] (purity: >98%; B2543), Mg[TFSA]$_2$ (purity: >97%; M2861), and Ca[TFSA]$_2$ (purity: >97%; C3263) were purchased from Tokyo Chemical Industry Co. Ltd. The experimental setup is described in a separate paper.[60] The TFSA powder sample (~300 mg) was placed in a Pt basket (ø 20 mm × 50 mm) hanging from a magnet, and the basket was suspended inside the furnace via the magnetic force. Before initiating the
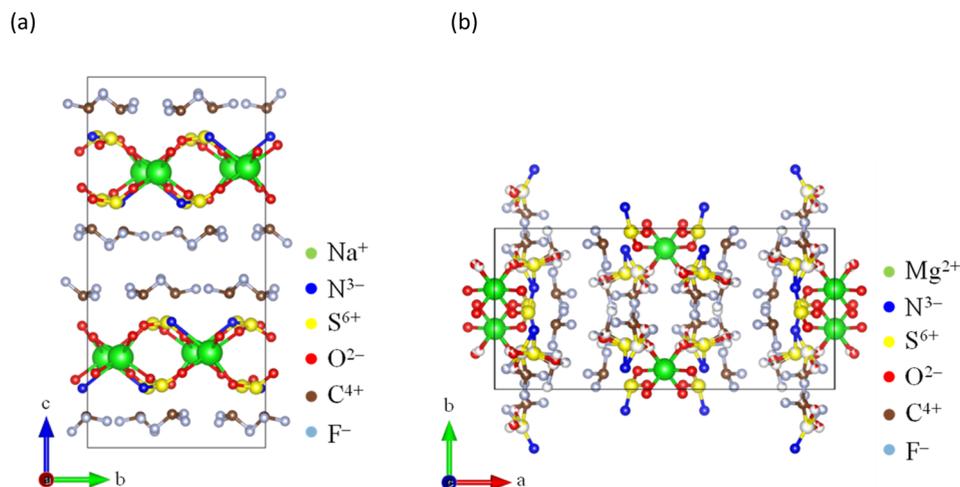
Fig. 1 Crystal structures of TFSA salts: (a) Na[TFSA][57] and (b) Mg[TFSA]$_2$.[59]

NH$_3$ absorption/desorption cycle, the TFSA sample was dehydrated at 493 K for 1 h under vacuum as pretreatment. After dehydration, pure NH$_3$ gas (99.9% purity; Resonac Holdings Corp., Tokyo, Japan) was introduced into the furnace. NH$_3$ absorption into the sample was conducted under a NH$_3$ gas pressure of 0.5 MPa for 2 h (pressure-swing absorption), whereas NH$_3$ desorption was conducted under a NH$_3$ gas pressure of 0.1 MPa for 3 h (pressure-swing desorption). The pressure of NH$_3$ was controlled by the temperature of the NH$_3$ tank immersed in an ethanol bath. After NH$_3$ absorption/desorption cycles, the sample powders were characterized using X-ray diffraction (XRD; Ultima IV, Rigaku Corp., Japan). XRD data were obtained in the 2θ range of 5–90° at room temperature, with a step interval of 0.01°, using Cu-Kα radiation, calibrated with Si powder. The obtained diffraction patterns were analysed *via* the entire powder pattern fitting method,[61,62] using PDXL (Rigaku Corp.) and split pseudo-Voigt functions. The corresponding crystal structures were visualized using VESTA.[63]

3   Results and discussion

3.1   Absorption and desorption behaviours of ammonia

Typical NH$_3$ absorption/desorption cycles for Na[TFSA] at 473 K are shown in Fig. 2. Na[TFSA] exhibits a stable NH$_3$ absorption capacity at 473 K and all pressures (0.1 and 0.5 MPa of NH$_3$ gas). The absorption capacity (C_{abs}) and desorption capacity (C_{des}) of NH$_3$ are defined as follows:

$$C_{abs} = \frac{W_{abs} - W_s}{W_s} \times \frac{1}{M_{NH_3}} \qquad (1)$$

$$C_{des} = \frac{|W_{des} - W_{abs}|}{W_s} \times \frac{1}{M_{NH_3}} \qquad (2)$$

where W_s is the sample weight before the NH$_3$ absorption/desorption cycle, W_{abs} is the sample weight after the absorption cycle, and W_{des} is the sample weight after the desorption cycle. M_{NH_3} is the molar weight of NH$_3$. The absorption/desorption rates (v_{abs} and v_{des}) are defined as the rates at which 80% of the capacity is achieved in each cycle. Na[TFSA] absorbs NH$_3$ ($C_{abs} = 3.05$ mmol g^{-1}) and exhibits the highest NH$_3$ desorption capacity ($C_{des} = 2.83$ mmol g^{-1}) among the four TFSA salts. This result indicates that almost all of the
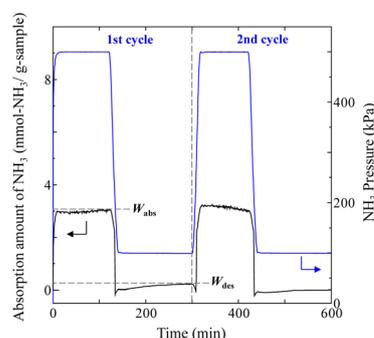

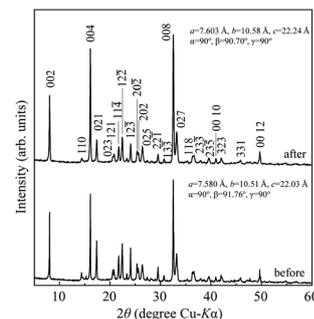Fig. 2 Typical NH$_3$ absorption/desorption cycles of Na[TFSA] at 473 K.

Fig. 3 XRD patterns of Na[TFSA] before and after NH$_3$ absorption/desorption cycles at 473 K.

absorbed NH$_3$ in Na[TFSA] can be collected *via* PSA. The XRD patterns of the Na[TFSA] powder before and after the NH$_3$ absorption/desorption cycles are shown in Fig. 3. The observed diffraction patterns are consistent with Na[TFSA] with a monoclinic $P2_1/n$ structure,[57] exhibiting crystal orientation and expansion along the c-axis after the absorption/desorption cycles. This result suggests that the NH$_3$ molecules are absorbed between the lattice layers of Na[TFSA]. As shown in Fig. 4, the NH$_3$ absorption behaviour varies based on the cation species of the TFSA salts. The results of the NH$_3$ absorption/desorption cycles for each TFSA sample are summarized in Table 2. Only a small amount of NH$_3$ is absorbed by K[TFSA] (Fig. 4a). Among the TFSA salts, Mg[TFSA]$_2$ exhibits the highest NH$_3$ absorption capacity ($C_{abs} = 8.29$ mmol g^{-1}) at 473 K, although the desorption capacity is low ($C_{des} = 1.22$ mmol g^{-1}) (Fig. 4b and Table 2). The C_{abs} values increase in the order of Mg[TFSA]$_2$ > Ca[TFSA]$_2$ > Na[TFSA]. This result is consistent with that reported by Liu and Aika.[23] They identified the absorption site of NH$_3$ and clarified the absorption mechanism with alkaline or alkaline-earth metal cations using a thermal conductivity detector and FT-IR spectroscopy. NH$_3$ is absorbed at these cation sites by three processes: coulombic attraction, the formation of ammonium ions, and the formation of ammine complexes in cation sites. Therefore, it is likely that NH$_3$ is absorbed at the alkaline or alkaline-earth metal cations of the TFSA salts. Based on the results of Liu and Aika,[23] NH$_3$ molecules are absorbed through the coulombic attraction between alkaline or alkaline-earth metal cations and the nitrogen anions of NH$_3$. Therefore, C_{abs} varies with the surface charge density of the alkaline or alkaline-earth metal cations. After the NH$_3$ absorption/desorption cycle at 473 K, the solid Mg[TFSA]$_2$ liquefies (Fig. 5b). This liquefaction decreases the NH$_3$ desorption from Mg[TFSA]$_2$. The XRD pattern of the solidified Mg[TFSA]$_2$ sample at room temperature is shown in Fig. 6a. The observed diffraction pattern is assigned to NH$_4$[TFSA] with an orthorhombic $Pnab$ structure[65] and Mg(NH$_2$)$_2$ with a cubic $I4_1/acd$:2 structure,[66] indicating that the Mg^{2+} cations are displaced by NH$_4^+$ cations as follows:

$$Mg[TFSA]_2 + 4NH_3 \rightarrow 2NH_4[TFSA] + Mg(NH_2)_2 \qquad (3)$$
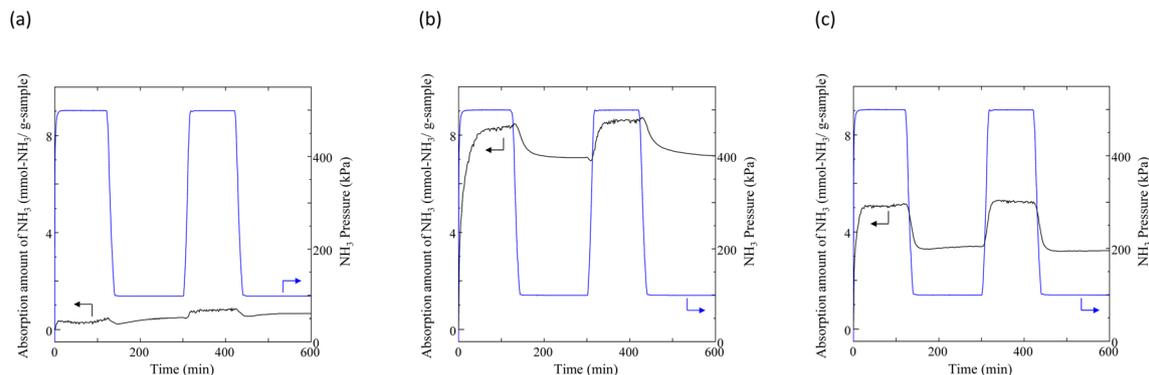
Fig. 4 Typical NH_3 absorption/desorption cycles for TFSA salts at 473 K: (a) K[TFSA], (b) Mg[TFSA]$_2$, and (c) Ca[TFSA]$_2$.

Table 2 NH_3 absorption/desorption measurements at 473 K

TFSA	Cycle	Absorption capacity, C_{abs} (mmol g^{-1})	Absorption rate, v_{abs} (mmol g^{-1} min^{-1})	Desorption capacity, C_{des} (mmol g^{-1})	Desorption rate, v_{des} (mmol g^{-1} min^{-1})
Na[TFSA]	1st	3.05	0.81	2.83	0.17
	2nd	3.03	0.19	3.03	0.20
Mg[TFSA]$_2$	1st	8.29	0.36	1.22	0.02
	2nd	8.66	—	1.51	0.02
Ca[TFSA]$_2$	1st	5.19	0.47	1.74	0.07
	2nd	5.18	0.32	1.95	0.09
Na–Y zeolite[a]	1st	5.08	4.14	2.18	0.10
	2nd	5.45	0.59	2.09	0.09

[a] The results of Na–Y zeolite were referred from ref. 64.

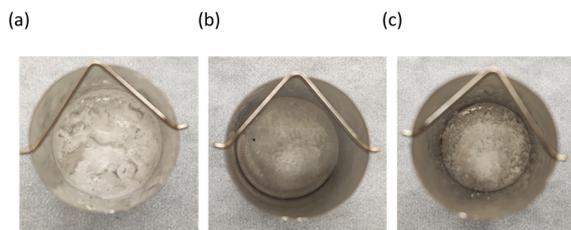**Fig. 5** Photographs of TFSA salts after the NH_3 absorption/desorption cycles at 473 K: (a) Na[TFSA], (b) Mg[TFSA]$_2$, and (c) Ca[TFSA]$_2$ in the Pt basket (ø 20 mm).

Liquefaction of solid salts that absorb excessive NH_3 has already been reported.[40,60,67] Ammonium (NH_4^+) cations and amide (NH_2^-) anions have been observed in bis(fluorosulfonyl) amide (FSA) salts after NH_3 absorption, and the FSA salts were liquefied by formation of a eutectic mixture among them.[60] Similarly, the liquefaction of the Mg[TFSA]$_2$ salt can be explained by a eutectic phenomenon. This indicates that the NH_3 molecule coordinates with the Mg^{2+} cation between the lattice layers and dissociates in the Mg[TFSA]$_2$ salt. Therefore, two absorption processes, coordination and dissociation, occur in Mg[TFSA]$_2$, as shown in Fig. 7. The XRD pattern of the Ca [TFSA]$_2$ sample shows phases of Ca[TFSA]$_2$,[57] NH_4[TFSA], and

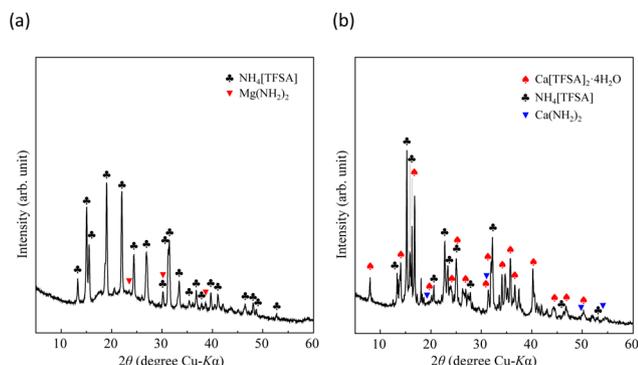**Fig. 6** XRD patterns of alkaline-earth metal TFSA salts after NH_3 absorption/desorption cycles at 473 K: (a) Mg[TFSA]$_2$ and (b) Ca[TFSA]$_2$.
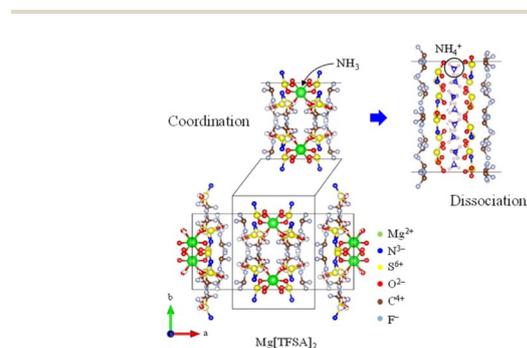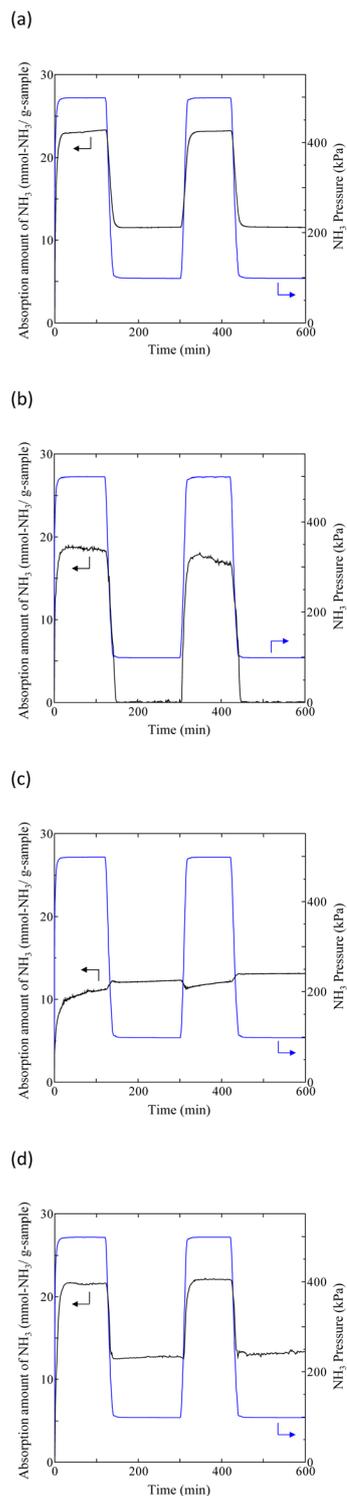

Fig. 7 Absorption mechanism of NH_3 into TFSA salt.

Fig. 8 Typical NH_3 absorption/desorption cycles in various TFSA salts at 300 K: (a) Na[TFSA], (b) K[TFSA], (c) Mg[TFSA]$_2$, and (d) Ca[TFSA]$_2$.

Ca(NH$_2$)$_2$ (ref. 68) (Fig. 6b). Therefore, in addition to Mg[TFSA]$_2$, the above mentioned two absorption processes occur in Ca[TFSA]$_2$. To evaluate the temperature dependence of the NH_3 absorption/desorption behaviour of the solid TFSA salts, NH_3

absorption/desorption cycles were examined at 300 K (Fig. 8 and Table 3). C_{abs} was higher at lower temperatures. At 300 K, Na [TFSA] exhibited the highest C_{abs}. K[TFSA] absorbed NH_3 under 0.5 MPa and showed the high desorption function of NH_3. All absorbed NH_3 was desorbed from K[TFSA] under 0.1 MPa. The difference of NH_3 absorption behaviours by temperature can be attributed to the NH_3 molecular motion. The NH_3 molecular motion was vigorous and C_{abs} decreased at high temperature (473 K). On the other hand, the absorbed NH_3 did not desorb from Mg[TFSA]$_2$ at 300 K (Fig. 8b). The crystal lattice of Na[TFSA] shrank after NH_3 absorption/desorption cycles at 300 K (Fig. 10a), implying that the Na[TFSA] lattice expanded during NH_3 absorption and shrank during NH_3 desorption. Mg[TFSA]$_2$ remained in the solid state after NH_3 absorption/desorption cycles at 300 K (Fig. 9). The XRD pattern of the Mg[TFSA]$_2$ sample after cycling at 300 K showed both Mg[TFSA]$_2$ and NH$_4$[TFSA] phases (Fig. 10b). The Mg^{2+} cations in Mg[TFSA]$_2$ were not entirely displaced by NH$_4^+$ cations. Therefore, the absorption process was limited by the dissociation of NH_3 in Mg [TFSA]$_2$ at 300 K. Regarding kinetics, the NH_3 absorption rate of Na[TFSA] was similar to its NH_3 desorption rate. Na[TFSA] exhibited the highest v_{abs} and v_{des} among the TFSA samples. v_{abs} and v_{des} values were higher at lower temperatures. In addition, although all TFSA salts except K[TFSA] showed similar NH_3 absorption behaviour at 473 K, they exhibited different behaviours at 300 K (Fig. 11). This was caused by the difference in the absorption processes; the absorption into the TFSA salts was limited by the dissociation of NH_3 in the salts. The double exponential model used to evaluate the kinetics of the two absorption processes is as follows:[69–71]

$$W(t) = A_{crd} \exp(-k_{crd}t) + A_{dis} \exp(-k_{dis}t) + C \tag{4}$$

where $W(t)$ is the change in sample weight over time t after the start of NH_3 absorption, and k_{crd} and k_{dis} are the rate constants for the coordination and dissociation of NH_3, respectively.

A_{crd} and A_{dis} are the frequency factors for the coordination and dissociation, respectively, and C is a constant. The first and second terms on the right side of eqn (4) correspond to the coordination and dissociation of NH_3 in the TFSA salts, respectively. The kinetic parameters were obtained by fitting the initial stage of the NH_3 absorption curves for each TFSA salt (Fig. 11a and c) using eqn (4), and the values are listed in Tables 4 and 5. The least-squares fitting results are shown in Fig. S1 and S2.† The rate constants of the coordination step are considerably higher than those of the dissociation step ($k_{crd} > k_{dis}$), confirming dissociation to be the rate-determining step. The value of k_{crd} increases and that of k_{dis} decreases with decreasing temperature. For Ca[TFSA]$_2$ at 300 K, k_{dis} is significantly small, suggesting that the dissociation of NH_3 in Ca [TFSA]$_2$ is slow at 300 K. Therefore, coordination is the dominant process, whereas dissociation progressed to a lesser extent in the Ca[TFSA]$_2$ salt.

3.2 Comparison of TFSA salts with zeolites

In our previous study,[64] NH_3 adsorption and desorption behaviours on zeolites at 473 K were observed by PSA cycling

Table 3 NH_3 absorption/desorption measurements at 300 K

TFSA	Cycle	Absorption capacity, C_{abs} (mmol g^{-1})	Absorption rate, v_{abs} (mmol g^{-1} min^{-1})	Desorption capacity, C_{des} (mmol g^{-1})	Desorption rate, v_{des} (mmol g^{-1} min^{-1})
Na[TFSA]	1st	23.34	3.61	11.77	0.53
	2nd	23.26	1.29	11.72	0.52
K[TFSA]	1st	18.48	2.56	18.37	0.63
	2nd	17.02	0.87	17.02	0.60
Ca[TFSA]$_2$	1st	21.64	2.05	8.92	0.57
	2nd	22.07	1.25	8.76	0.57

Fig. 9 A photograph of the Mg[TFSA]$_2$ sample after NH_3 absorption/desorption cycles at 300 K. Mg[TFSA]$_2$ sample in the glass bottle (ø 24 mm, 10 mL).
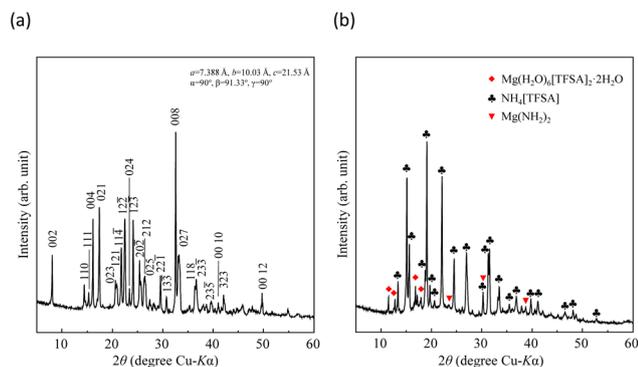

Fig. 10 XRD patterns of TFSA salts after NH_3 absorption/desorption cycles at 300 K: (a) Na[TFSA] and (b) Mg[TFSA]$_2$.

(0.1–0.5 MPa), and their stability for NH_3 storage was confirmed. Typical NH_3 adsorption and desorption behaviours of Na–Y and A-4 zeolites at 473 K are shown in Fig. S3.† As shown in Table 2, although the NH_3 adsorption capacity of the Na–Y zeolite (C_{ads} = 5.08 mmol g^{-1}, 7.16 mol m^{-3}) is higher than that of Na[TFSA] (C_{abs} = 3.05 mmol g^{-1}, 7.13 mol m^{-3}), the NH_3 desorption capacity of the Na–Y zeolite (C_{des} = 2.18 mmol g^{-1}, 3.07 mol m^{-3}) is lower than that of Na[TFSA] (C_{des} = 2.83 mmol g^{-1}, 6.62 mol m^{-3}). Additionally, the NH_3 desorption rate of Na–Y zeolite (v_{des} = 0.10 mmol g^{-1} min^{-1}) is lower than that of the Na[TFSA] salt (v_{des} = 0.17 mmol g^{-1} min^{-1}). Hence, the NH_3 desorption function of the Na–Y zeolite is less than that of Na[TFSA]. These results indicate that zeolites contain non-collectible NH_3 during this PSA cycle (0.1–0.5 MPa, collection ratio: 43%). In contrast, almost all the NH_3 absorbed by the Na[TFSA] salt is collected (collection ratio: 93%). Therefore, the high NH_3 desorption function is an advantage of NH_3 separation using TFSA salts. Finally, to evaluate the durability of the Na[TFSA] for NH_3 absorption/desorption at 473 K, five NH_3 absorption/desorption cycles were conducted (Fig. 12a). Stable NH_3 absorption/desorption behaviours were observed, although the baseline of balance was drifted by multiple changes in NH_3 pressure. From the cycle performance of the NH_3 desorption capacity as a working capacity (Fig. 12b), it was confirmed that Na[TFSA] absorbed and desorbed NH_3 in stably and repeatably. Furthermore, even after five NH_3 absorption/desorption cycles, Na[TFSA] remained as a sold-state and no other compounds such as NH$_4$[TFSA] were observed (Fig. 12c). From these results, the durability of the Na[TFSA] was confirmed for NH_3 absorption/desorption at 473 K.
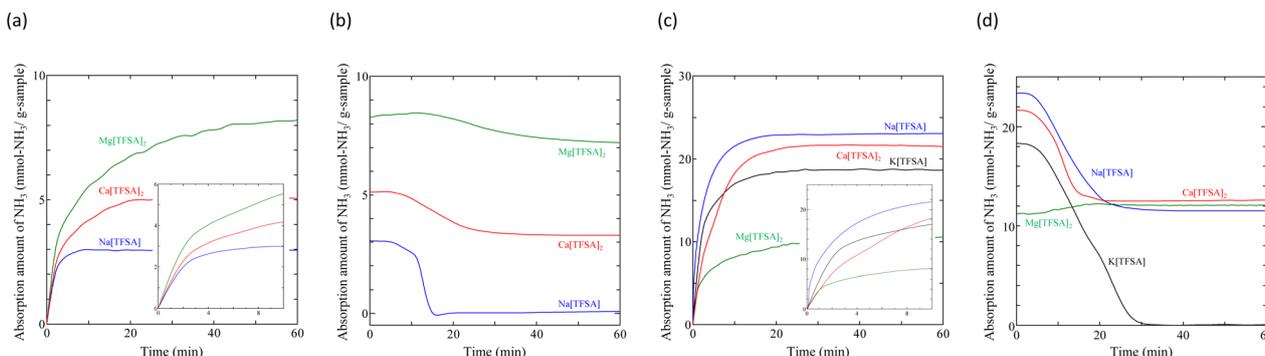

Fig. 11 Initial stages of NH_3 absorption/desorption of TFSA salts: (a) absorption at 473 K, (b) desorption at 473 K, (c) absorption at 300 K, and (d) desorption at 300 K.

Table 4 Kinetic parameters of NH_3 absorption into TFSA salts at 473 K

TFSA	A_{crd}	A_{dis}	C	$k_{crd} \times 10^{-3}$ (s^{-1})	$k_{dis} \times 10^{-3}$ (s^{-1})	R^2
Na[TFSA]	−2.13927	−2.85738	4.996652	47.22	6.248	0.9994
Mg[TFSA]$_2$	−3.44905	−7.41104	10.86009	78.91	2.623	0.9994
Ca[TFSA]$_2$	−2.75006	−5.69369	8.44375	62.09	2.520	0.9991

Table 5 Kinetic parameters of NH_3 absorption into TFSA salts at 300 K

TFSA	A_{crd}	A_{dis}	C	$k_{crd} \times 10^{-3}$ (s^{-1})	$k_{dis} \times 10^{-3}$ (s^{-1})	R^2
Na[TFSA]	−10.4859	−27.7007	38.1866	57.22	4.742	0.9999
K[TFSA]	−16.5615	−20.9808	37.5423	19.48	1.188	0.9997
Mg[TFSA]$_2$	−7.29562	−9.26933	16.54037	242.0	2.128	0.9967
Ca[TFSA]$_2$	−7.03838	−59.9431	66.89941	299.2	0.893	0.9996
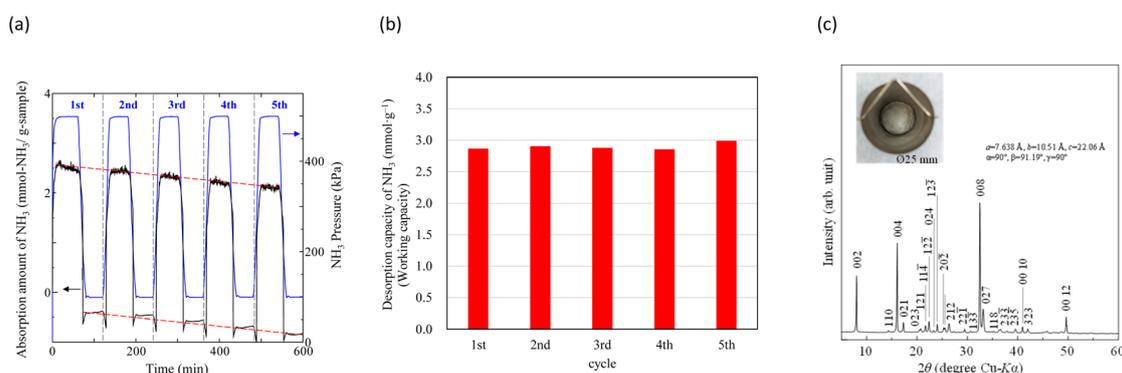
Fig. 12 The results of NH_3 absorption/desorption cycles (5 cycles) of Na[TFSA] at 473 K. (a) NH_3 absorption/desorption curves, (b) cycle performance of working capacity, and (c) the XRD pattern of the Na[TFSA] sample after five NH_3 absorption/desorption cycles.

4 Conclusions

The NH_3 absorption and desorption behaviours of TFSA salts were investigated using PSA. The effects of the cation species and temperature on the NH_3 absorption behaviour were evaluated for four TFSA salts: Na[TFSA], K[TFSA], Mg[TFSA]$_2$, and Ca[TFSA]$_2$. NH_3 was absorbed by all of these solid TFSA salts. Among them, Na[TFSA] at 473 K and K[TFSA] at 300 K exhibited high NH_3 desorption ability, with NH_3 desorption capacities of 2.83 and 18.37 mmol g^{-1} and collection ratios of 93 and 99%, respectively. The NH_3 absorption behaviour depended on the cation species of the TFSA salt. Crystallographic refinement showed that the crystal lattice of Na[TFSA] expanded and contracted along the c-axis during NH_3 absorption and desorption, respectively, suggesting high desorption of NH_3 molecules from the lattice layers. For alkaline-earth metal TFSA salts, NH_4[TFSA] and amide compounds ($Mg(NH_2)_2$ or $Ca(NH_2)_2$) were formed after NH_3 absorption. This indicated that NH_3 dissociated in solid TFSA salts. Therefore, two absorption processes, namely, coordination and dissociation of NH_3, occurred in the solid TFSA salts. Kinetic analysis confirmed that NH_3 dissociation was the rate-determining step for NH_3 storage in the salts.

Data availability

The data supporting this article have been included as part of the ESI.†

Author contributions

M. T.: investigation, data curation, visualization, writing – original draft. R. F.: investigation, data curation. J. R.: supervision, funding acquisition, writing – review and editing, revision and suggestions. All the authors participated in discussions of the results and in preparing the manuscript.

Conflicts of interest

There are no conflicts to declare.

Acknowledgements

References

1 J. W. Erisman, M. A. Sutton, J. Galloway, Z. Klimont and W. Winiwarter, *Nat. Geosci.*, 2008, **1**, 636.

2 A. Valera-Medina, H. Xiao, M. Owen-Jones, W. I. F. David and P. J. Bowen, *Prog. Energy Combust. Sci.*, 2018, **69**, 63.

3 K. E. Lamb, M. D. Dolan and D. F. Kennedy, *Int. J. Hydrogen Energy*, 2019, **44**, 3580.

4 D. R. MacFarlane, P.-V. Cherepanov, J. Choi, B. H. R. Suryanto, R. Y. Hodgetts, J. M. Bakker, F. M. F. Vallana and A. N. Simonov, *Joule*, 2020, **4**, 1186.

5 M. Ravi and J. W. Makepeace, *Chem. Sci.*, 2022, **13**, 890.

6 S. Sun, Q. Jiang, D. Zhao, T. Cao, H. Sha, C. Zhang, H. Song and Z. Da, *Renewable Sustainable Energy Rev.*, 2022, **169**, 112918.

7 P. Mayer, A. Ramirez, G. Pezzella, B. Winter, S. M. Sarathy, J. Gascon and A. Bardow, *iScience*, 2023, **26**, 107389.

8 K. Aika, H. Hori and A. Ozaki, *J. Catal.*, 1972, **27**, 424.

9 K. Aika, *Angew Chem. Int. Ed. Engl.*, 1986, **25**, 558.

10 K. Aika and T. Kakegawa, *Catal. Today*, 1991, **10**, 73.

11 K. Aika and H. Kobayashi, *CO₂ Free Ammonia as an Energy Carrier*, Springer, Singapore, 2023.

12 J. Guo and P. Chen, *Chem*, 2017, **3**, 709.

13 Q. Wang, J. Guo and P. Chen, *J. Energy Chem.*, 2019, **36**, 25.

14 H. Liu, *Chin. J. Catal.*, 2014, **35**, 1619.

15 P. Wang, F. Chang, W. Gao, J. Guo, G. Wu, T. He and P. Chen, *Nat. Chem.*, 2016, **9**, 64.

16 R. Shi, X. Zhang, G. I. N. Waterhouse, Y. Zhao and T. Zhang, *Adv. Energy Mater.*, 2020, **10**, 2000659.

17 C. Y. Liu and K. Aika, *Chem. Lett.*, 2002, **31**, 798.

18 C. Y. Liu and K. Aika, *Ind. Eng. Chem. Res.*, 2004, **43**, 7484.

19 C. Y. Liu and K. Aika, *Bull. Chem. Soc. Jpn.*, 2004, **77**, 123.

20 C. Y. Liu and K. Aika, *Ind. Eng. Chem. Res.*, 2004, **43**, 6994.

21 C. Y. Liu and K. Aika, *Res. Chem. Intermed.*, 2002, **28**, 409.

22 C. Y. Liu and K. Aika, *Bull. Chem. Soc. Jpn.*, 2003, **76**, 1463.

23 C. Y. Liu and K. Aika, *J. Jpn. Pet. Inst.*, 2003, **46**, 301.

24 M. Malmali, Y. Wei, A. McCormick and E. L. Cussler, *Ind. Eng. Chem. Res.*, 2016, **55**, 8922.

25 M. Malmali, G. Le, J. Hendrickson, J. Prince, A. V. McCormick and E. L. Cussler, *ACS Sustainable Chem. Eng.*, 2018, **6**, 6536.

26 M. Malmali, M. Reese, A. V. McCormick and E. L. Cussler, *ACS Sustainable Chem. Eng.*, 2018, **6**, 827.

27 C. Smith, M. Malmali, C. Liu, A. V. McCormick and E. L. Cussler, *ACS Sustainable Chem. Eng.*, 2018, **6**, 11827.

28 D. K. Ojha, M. J. Kale, A. V. McCormick, M. Reese, M. Malmali, P. Dauenhauer and E. L. Cussler, *ACS Sustainable Chem. Eng.*, 2019, **7**, 18785.

29 B. Lin, T. Wiesner and M. Malmali, *ACS Sustainable Chem. Eng.*, 2020, **8**, 15517.

30 B. Lin, F. H. Nowrin, J. J. Rosenthal, A. S. Bhown and M. Malmali, *ACS Sustainable Chem. Eng.*, 2023, **11**, 9880.

31 C. E. Onuoha, M. J. Kale, M. Malmali, P. J. Dauenhauer and A. V. McCormick, *Ind. Eng. Chem. Res.*, 2024, **63**, 5608.

32 E. W. Washburn, *International Critical Tables of Numerical Data, Physics, Chemistry and Technology 7*, McGraw-Hill, NY, 1929.

33 A. Yokozeki and M. B. Shiflett, *Ind. Eng. Chem. Res.*, 2007, **46**, 1605.

34 T. Aoki, T. Ichikawa, H. Miyaoka and Y. Kojima, *J. Phys. Chem. C*, 2014, **118**, 8412.

35 Y. Kojima and M. Yamaguchi, *Int. J. Hydrogen Energy*, 2020, **45**, 10233.

36 H. Chu, G. Wu, Z. Xiong, J. Guo, T. He and P. Chen, *Chem. Mater.*, 2010, **22**, 6021.

37 M. J. Kale, D. K. Ojha, S. Biswas, J. I. Militti, A. V. McCormick, J. H. Schott, P. J. Dauenhauer and E. L. Cussler, *ACS Appl. Energy Mater.*, 2020, **3**, 2576.

38 C. Shen, P. Wang, L. Shen, X. Yin and Z. Miao, *Ind. Eng. Chem. Res.*, 2022, **61**, 8616.

39 W. Q. Gong, Y. X. Fu, Y. Zhou, M. S. Sun, Z. M. Li, N. H. Lu and D. J. Tao, *Sep. Purif. Technol.*, 2023, **322**, 124304.

40 K. Zong and D. Deng, *Sep. Purif. Technol.*, 2024, **349**, 127869.

41 Y. Cao, K. Jiang and D. Deng, *Sustainable Energy Fuels*, 2024, **8**, 3933.

42 J. Foropoulos and D. D. DesMarteau, *J. Am. Chem. Soc.*, 1982, **104**, 4260.

43 J. Foropoulos and D. D. DesMarteau, *J. Fluorine Chem.*, 1982, **21**, 9.

44 L. Xue, D. D. DesMarteau and W. T. Pennington, *Angew Chem. Int. Ed. Engl.*, 1997, **36**, 1331.

45 P. Johansson, S. P. Gejji, J. Tegenfeldt and J. Lindgren, *Electrochim. Acta*, 1998, **43**, 1375.

46 A. Yokozeki and M. B. Shiflett, *Appl. Energy*, 2007, **84**, 1258.

47 W. Shi and E. J. Maginn, *AIChE J.*, 2009, **55**, 2414.

48 J. Palomar, M. Gonzalez-Miquel, J. Bedia, F. Rodriguez and J. J. Rodriguez, *Sep. Purif. Technol.*, 2011, **82**, 43.

49 J. Bedia, J. Palomar, M. Gonzalez-Miquel, F. Rodriguez and J. J. Rodriguez, *Sep. Purif. Technol.*, 2012, **95**, 188.

50 Y. Li, M. C. Ali, Q. Yang, Z. Zhang, Z. Bao, B. Su, H. Xing and Q. Ren, *ChemSusChem*, 2017, **10**, 3368.

51 F. Zhong, H. Peng, D. Tao, P. Wu, J. Fan and K. Huang, *ACS Sustainable Chem. Eng.*, 2019, **7**, 3258.

52 A. Finotello, J. E. Bara, D. Camper and R. D. Noble, *Ind. Eng. Chem. Res.*, 2007, **47**, 3453.

53 M. Ramdin, T. W. de Loos and T. J. H. Vlugt, *Ind. Eng. Chem. Res.*, 2012, **51**, 8149.

54 M. Ramdin, S. P. Balaji, J. M. Vicent-Luna, J. J. Gutiérrez-Sevillano, S. Calero, T. W. de Loos and T. J. H. Vlugt, *J. Phys. Chem. C*, 2014, **118**, 23599.

55 A. Rivera-Pousa, R. Lois-Cuns, M. Otero-Lema, H. Montes-Campos, T. Méndez-Morales and L. Miguel Varela, *J. Chem. Inf. Model.*, 2024, **64**, 164.

56 L. Xue, D. D. DesMarteau and W. T. Pennington, *Solid State Sci.*, 2005, **7**, 311.

57 K. Matsumoto, T. Matsui, T. Nohira and R. Hagiwara, *J. Fluorine Chem.*, 2015, **174**, 42.

58 L. Xue, C. W. Padgett, D. D. DesMarteau and W. T. Pennington, *Solid State Sci.*, 2002, **4**, 1535.

59 G. Veryasov, U. Harinaga, K. Matsumoto and R. Hagiwara, *Eur. J. Inorg. Chem.*, 2017, **2017**, 1087.

60 M. Tokushige, R. Fujisawa and J. Ryu, *Sustainable Energy Fuels*, 2024, **8**, 397.

61 G. S. Pawley, *J. Appl. Crystallogr.*, 1981, **14**, 357.

62 H. Toraya, *J. Appl. Crystallogr.*, 1986, **19**, 440.

63 K. Momma and F. Izumi, *J. Appl. Crystallogr.*, 2011, **44**, 1272.

64 M. Tokushige and J. Ryu, *ACS Omega*, 2023, **8**, 32536.

65 M. G. Davidson, P. R. Raithby, A. L. Johnson and P. D. Bolton, *Eur. J. Inorg. Chem.*, 2003, **2003**, 3445.

66 H. Jacobs, *Z. Anorg. Allg. Chem.*, 1971, **382**, 97.

67 L. Gao, H. Fang, Z. Li, X. Yu and K. Fan, *Inorg. Chem.*, 2011, **50**, 4301.

68 R. Juza and H. Schumacher, *Z. Anorg. Allg. Chem.*, 1963, **324**, 278.

69 N. Koga, Y. Goshi, S. Yamada and L. A. Pérez-Maqueda, *J. Therm. Anal. Calorim.*, 2013, **111**, 1463.

70 İ. Tosun, *Int. J. Environ. Res. Public Health*, 2012, **9**, 970.

71 V. Kiss and K. Ősz, *Int. J. Chem. Kinet.*, 2017, **49**, 602.